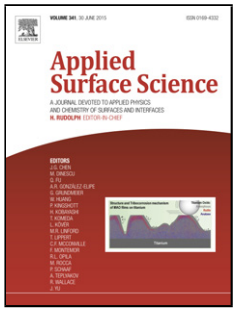

Title: Spectroscopic characterization and docking studies of ZnO nanoparticle modified with BSA

Authors: Ana E. Ledesma, Doly María Chemes, María de los Angeles Frías, Maria del Pilar Guauque Torres

PII: S0169-4332(17)30894-2
DOI: http://dx.doi.org/doi:10.1016/j.apsusc.2017.03.202
Reference: APSUSC 35578

To appear in: *APSUSC*

Received date: 28-12-2016
Revised date: 21-3-2017
Accepted date: 22-3-2017

Please cite this article as: Ana E.Ledesma, Doly María Chemes, María de los Angeles Frías, Maria del Pilar Guauque Torres, Spectroscopic characterization and docking studies of ZnO nanoparticle modified with BSA, Applied Surface Sciencehttp://dx.doi.org/10.1016/j.apsusc.2017.03.202

<AT>Spectroscopic characterization and docking studies of ZnO nanoparticle modified with BSA.

<AU>Ana E. Ledesma[a*] anael@unse.edu.ar; Doly María Chemes[b]; María de los Angeles Frías[c]; Maria del Pilar Guauque Torres[a]
<AFF>[a]CITSE-UNSE, CONICET, FCEyT, RN 9, km 1125, (4206) Santiago del Estero, Argentina
<AFF>[b]INQUINOA, UNT, CONICET, FBQyF, San Lorenzo 456, San Miguel de Tucumán CPA T4000ILI, Tucumán, Argentina
<AFF>[c]Laboratory of Biointerphases and Biomimetic Systems, (CITSE) National University of Santiago del Estero and CONICET, 4206, RN 9- Km 1125, Santiago del Estero, Argentina
<PA>Tel.: +54385 4509560.

<ABS-HEAD>Highlights► The ZnO NPs have synthesized at moderate temperature and conjugated with BSA to elucidate the characteristics of best binding site in the protein cavity. ► The Docking studies have successfully applied to identify the amino acids residues involved in the interaction. ► The cytotoxicity of ZnO NPs and ZnO-BSA NPs and esterase-like activity of the protein have evaluated, with very promising results for medical applications.

<ABS-HEAD>Abstract

<ABS-P>*Nanoparticles (NP) into a biological environment are an interesting topic for diagnosis and therapy in applications for medicine or environment and the knowledge about this interaction is important from the perspective of safe use of nanomaterials.* In the current study, we characterized the type of interaction and the orientation of *bovine serum albumin* (BSA) adsorbed on ZnO nanoparticle surfaces as a function of size, using molecular docking. To probe experimentally different theoretical hypothesis about the interaction, ZnO-NPs were prepared in aqueous solution, and then were bioconjugated with BSA. *Transmission electron microscopy* (TEM) and Raman spectroscopy confirm the spherical shape of NP and the irreversible adsorption of BSA on NP surface. Raman and Infrared spectroscopy (FTIR) reveal that BSA interaction with ZnO nanoparticle produced a conformational rearrangement into protein, observing changes in Tyr and Trp environment, a minor percentage of α-helix structure and a more extended chain. The fluorescence analysis demonstrated that when BSA concentration higher than 30 μM is used the signal due to the self-oligomerization of protein overlaps with the ZnO nanoparticle emission. The results predicted that the most probable interaction site is near to domain IB and IIA and ionic interactions are the major responsible for the binding. Thermal stability studies reveals that the denaturalization temperature of BSA increase from *57°C to 65* ºC in presence of ZnO NP and their esterase-like activity was improved.

<KWD>Keywords: ZnO nanoparticles; BSA protein; molecular docking; FTIR and Raman spectroscopic; thermal stability; esterase-like activity.

〈H1〉1. Introduction

In the last years, nanotechnology has developed with the purpose to obtain NP (NPs) with functional properties for biomedical applications and diagnostics[1–3]. Using nano-engineering, the NP with similar size as biological molecules, can be localized in any system of the body and to interact with biomolecules modifying their activity into the biological system. The interaction of NPs with a biological environment, it makes it is covered a layer of proteins, forming what is known as the protein ``corona'' and as a consequence new properties can be observed [4]. Thus,

the transport of nanoparticle through the blood plasma to different parts of the body involves the retention of biomolecules on its surface with a significant biological impact, which depends on size and structure of NP in the solution as well as the affinity of the protein towards the NP surface. The way in which protein molecules arrange themselves on the NP surface may affect the biological reactivity of the latter at the cellular level [4]. The blood plasma is a mixture of the different biological components, in special proteins such as albumin, globulin and fibrinogen [5]. Among them, albumin represents an attractive macromolecular carrier that has been selected as a protein model to demonstrate its interaction with charged NP. In this sense Bovine serum albumin (BSA) has been used. This protein, which molecular weight is 66,000 Da, contains 20 tyrosine residues, 30 phenylalanine residues and 2 tryptophan (Trp134 and Trp213) with high helical content [6]. It binds with various molecules such as fatty acids, amino acids, steroids, metal ions, carbohydrates and other molecules [7].

ZnO NPs are widely investigated for their semiconductor properties that make it useful for application such as biosensors of great interest for biomedical and images diagnostic [8–12]. These NPs show high biocompatibility and cytotoxicity selective against cancerous cells in vitro condition compared with other NP [13].

Studies have demonstrated conformational changes when BSA interacts with ZnO NPs being the electrostatic forces the main contribution of this interaction [5,6] and the NPs-protein complex formation, reduces ZnO NPs cytotoxicity in vitro and ROS generation [7]. *However, the properties of binding site and conformational changes of protein by interaction with ZnO NP has been barely studied. For this reason, the aim of this research is to provide more details about formation of BSA-ZnO NP, characteristics of the binding site and the dominant interactions between protein and ZnO NP using computational docking studies and spectroscopic characterization. An evaluation of biological development of the protein after ZnO NPs interaction, showing its consequences on the optical properties of ZnO NPs and BSA structure as a major component in the bloodstream. This knowledge is important from the perspective of safe use of nanomaterials [1]. To our knowledge, this is the first time that computational docking studies were done to investigate the dominant interactions between protein and ZnO NP in order to bring complementary information for the application of this nanoparticles in biotechnological, medicinal, and pharmaceutical fields.*

<H1>2. Materials and methods

<H2>2.1.Chemical reagents

Zinc nitrate hexahydrate (Aldrich 98%), Bovine Serum Albumin lyophilized powder, Essentially fatty acids free (sigma-aldrich 99%), sodium phosphate monobasic monohydrate (J. T. Baker), *p*-nitrophenyl acetate (sigma-aldrich 98%), Sodium phosphate dibasic 12-Hydrated (J. T. Baker) and sodium hydroxide (Anedra 96%) were used without further purification. Ultrapurified distilled water was used for the preparation of all solution.

<H2>2.2. Preparation of nanoparticles

Zinc Oxide NP were synthesized using published procedures with same improves [14]. 0.9 M NaOH and 0.45 M $Zn(NO_3)_2.6H_2O$ solutions were prepared in ultrapurified water and filtered (0.22 µm Millipore filter). 5 mL of NaOH solution were heated at 55 °C in a bath water under constant stirring. When this temperature was achieved, Zinc Nitrate solution was slowly added (dropwise for 50 min) to the alkali solution into the glass flask, under continual stirring. After 2 h reaction, the white precipitate deposited in the bottom of the flask, was collected and washed several times with absolute ethanol and distilled water and then centrifuged. Finally, the ZnO NP were obtained after dehydration of the precipitate in air atmosphere at about 60 °C for two days.

Then, the solid previously obtained was suspended in ultrapurified water (1 mg/ml) and sonicated in an ultrasound bath during 30 min before each experiments to mix and form a homogeneous suspension.

For studying the interaction between ZnO NPs and BSA protein, appropriated aliquots of 500 µM stock solution of BSA in 10 mM phosphate buffer (pH =7.4), were used to arrive at the desired concentration for each experiments. BSA concentrations were calculated from their absorption at 280 nm using an extinction coefficient of 43,840 cm^{-1} M^{-1}.
Finally, 30 mg ZnO dried were suspended in 3mL of 5µM BSA (pH=7.4, phosphate Buffer 10 mM). The ZnO-BSA NPs mixture was incubated 2 hs with continue stirring at room temperature After that, the mixture was centrifuged 15 min at 3000 rpm, the supernatant was discarded and precipitate was washed using ultra purified water and centrifuged in the same conditions. This procedure was repeated three times. The pellets were dried at 50°C for one day and this solid was conserved at room temperature.

<H2>2.3. Characterization

The X-ray diffraction pattern for the ZnO NPs was recorded using an X-ray diffractometer RIGAKU D-MAX IIIC model operated at a voltage of 30 kV and current of 20 mA with a Cu radiation and Ni filter with 2 °/min of rate.
The morphology of ZnO structures was examined using a Jeol 100 CX II transmission electron microscope (TEM). Previously sonicated ZnO aqueous solution (1mg/mL) was deposited on a *Cu* grid at room temperature. To evaluate the ZnO NPs with BSA, 1 mg of ZnO NPs was suspended in 1mL of 5 µM BSA solution before prepared. *The obtained images were processed with Image J software with approximately 70 particles observed in 7 TEM images*

<H2>2.4. UV-Vis and Fluorescence measurement

UV-Vis absorption spectra were registered with a Hewlett Packard 8453 UV-visible spectrophotometer (Palo Alto, CA, USA). *The fluorescence excitation and emission spectra were recorded with a Hitachi F-2500 spectrofluorometer (Kyoto, Japan) equipped with an R-928 photomultiplier, in a fluorescence quartz cell of 1 cm of optical path (Hellma, Müllheim, Germany).*
For the ZnO NPs characterization, solid state and aqueous solution ZnO NPs were excited at 370 nm, the spectra were collected using excitation and emission width slits of 5 and 10 nm, respectively. The absorption spectrum of a suspension containing ZnO NPs (2 mM in water) was recorded, and then appropriate aliquots of BSA solution in phosphate buffer (pH=7.4) were successively added to cover a range of protein concentration up to 140 µM. The corresponding fluorescence spectra (λ_{exc}=370 nm and 340 nm) was performed using those solutions in the slit conditions above mentioned. BSA emission spectra were collected by excitation at 295 nm and 280 nm in order to evaluate the Trp and Tyr residues emissions respectively. The Trp fluorescence quenching, elicited by ZnO NPs addition, was recorded with excitation and emission slits width 2.5 nm of bandwidth.
All the measurements were recorded with a continued stirring, and for protein solutions, 5 min of incubation was allowed before the acquisition of the spectrum. A long-pass filters series (KV-389, KV-418 and KV 500) were used to select the UV and visible bands. In order to reduce primary and secondary inner filter effects, all the observed emission spectra were corrected using every absorption spectrum. Thus, emission intensities were corrected take into account the light absorption by ZnO NPs at 295 nm and 340 nm.

The quantity of adsorbed BSA on ZnO NP surface was evaluate using a 0.5 cm quartz cell according to the procedure proposed by Sotnikov et al. [15] using 480 µM ZnO NPs and BSA in the 0-15 µM range concentration. These results were obtained from the residual fluorescence of the reaction solution after separation from NP by centrifugation.

For thermal stability experiments, a mixture containing 2 mL of BSA (5 µM) with 100 µM of ZnO was placed in a thermostated cell of 1 cm of optical path and then incubated over a wide temperature range from 24°C to 84°C. In order to determine the influence of ZnO NPs on the BSA denaturation, temperature-dependent spectra at regular intervals were carried out. After 10 min at each temperature for thermal equilibrium, the fluorescence emission spectra with excitation at 280 nm and 295 nm using 5 and 10 nm slit excitation and emission were recorded.

<H2>2.5. FTIR and Raman studies

In order to investigate the BSA structural changes by ZnO NP interaction, Attenuated Total Reflectance Fourier transform infrared (ATR-FTIR) spectra were recorded on a Thermo Nicolet 6700 spectrometer equipped with a DTGS KBr detector, and KBr beam splitter. Measurements were obtained using the AMTIR crystal element in a horizontal ATR cell (Thermo Nicolet, Inc.). For solid nanoparticles (ZnO NP and ZnO-BSA NP complex), 1 mg of each sample was placed on crystal. For a liquid solution, a thin film of sample was prepared by depositing a BSA solution (30 µM in 10 mM phosphate buffer, pH 7.4) without and with 100 µM ZnO suspension) onto the AMTIR crystal and dried for 1 h before recording the spectra. In the same way, ATR-FTIR spectra of the thin films of nanoparticles in water were recorded.

FTIR spectra were processed using OPUS version 7.0 software. Fourier self-deconvolution and second derivative resolution enhancement were applied to narrow the widths of infrared bands and increase the separation of the overlapping components.

Raman spectra between 3500 and 50 cm-1 were collected using a DXR Raman Microscope (Thermo Fisher Scientific). Data were collected using a diode-pump solid state laser of 532 nm (5 cm-1 spectral resolution). A confocal aperture of 50 µm slit was used. A 10× objective was used by collecting Raman data. A single drop of each sample solution (230 µM BSA in buffer and 230 µM-1 of BSA in 1 mg/mL ZnO in buffer) was placed on gold-coated sample slides. In order to achieve a sufficient signal-to-noise ratio, 80 expositions with an exposure time of 6 s were accumulated for all samples. The laser power used was 10 mW.

<H2>2.6. Dynamic light scattering

The hydrodynamic diameters of ZnO NP with and without BSA were measured in a DLS SZ-100 Horiba. The powder nanoparticles (ZnO NP and ZnO-BSA complex) were dispersed in water (120 µM). The detection angle was 173°. For each sample, DLS measurements were conducted with a fixed 20 runs and each run lasts 30 seconds.

<H2>2.7. Esterase- Like activity

The BSA transport properties were evaluated through of esterase-like activity, in presence and absence of ZnO NP (0-120 µM), using *p*-nitrophenyl acetate (*p*-NPA) by following the formation of *p*-nitrophenol at 405 nm for 10 min. The reaction mixtures containing 50 µM *p*-nitrophenyl acetate and 20 µM protein in 0.1 M phosphate buffer pH 7.4, was monitored at 405 nm and using a molar extinction coefficient for p-nitrophenol of $\varepsilon = 17{,}700\ M^{-1}\ cm^{-1}$. One unit of esterase activity was defined as the quantity of enzyme required for release 1 µM of *p*-nitrophenol per minute at 25 °C. Esterase-like activity using different BSA concentration was measured in presence of 30 µM ZnO NPs. The BSA-ZnO incubation time-dependence was also evaluated.

<H2>2.8. Effect of ZnO-BSA NP complex on Hemolysis activity

The hemolytic effect of the ZnO NP was evaluated using washed erythrocytes (RBC) on human blood [16]. 10 ml of blood was mixing with the same quantity of EDTA solution and them was centrifuged during fifteen minutes. The obtained pellet was suspended in 10 ml of physiological saline solution, washed tree times and them centrifuged. 1 mg of ZnO and ZnO-BSA NPs respectively, were dispersed in 2 ml of suspended RBC and incubated for 90 min at 37 ºC with gentle shake. The mixture was centrifuged at 3000 rpm for 15 min and the absorption of the supernatant was measured at 540 nm.

<H2>2.9. Molecular Docking

In order to have a more detailed insight into the ZnO NPs-BSA interaction, we have estimated by molecular docking the possible site for NPs-protein association process, in agreement to the approach investigated by Khan et.al.[17]

Taking into account the experimental crystal lattice parameters obtained from literature [18], four different molecular structures with diameters from 14 Å to 30 Å were constructed. Different surfaces were visualized using GaussView 5.0 software [19] from crystal structure file of mineral zincite belonging to the wurtzite structure type with lattice parameters of a = 3.2489 Å and c = 5.2053 Å [18]. In order to obtain the appropriate structures, the lattice parameters has been increased from initial unit cell since one, two or three dimension. *To this purpose, two flat ZnO NPs surfaces (37 Å x 23 Å and 15 Å x 25 Å) and two 3D clusters mimicking the particle curvature of a ZnO NP were constructed*. All ZnO structures were generated using the GaussView software and Gaussian09 program package [20]. The surfaces were optimized using MGL Tools 1.5.6 by adding Marsilli-Gasteiger partial charges on each constituent atom. The surface diameters were estimated using VEGA ZZ Support Pack [21]. After this step, those structures were used as input for docking calculations.

Molecular docking studies were carried out using AutoDock 4.2 tool [22], with a semiempirical free-energy force. The crystal structure of BSA was obtained from Protein Data Bank (PDB ID: 4F5S), the PEG and water molecules were removed and then polar hydrogen atoms were added and assigning Kollman united atom charges was realized. In order to ensure that the free movement of all structures around the protein, docking studies were carried out considering a large grid volume (126 x 126 x 126 with 1 Å grid spacing) covering the all surface of the BSA to find the binding regions. The ligands and protein were treated as rigid docking. Default AutoDock parameters with Lamarckian Genetic Algorithm, a population of 150, number of GA runs of 100 and maximum number of generation of 27,000 for each experiments were used. All other parameters were default settings. Finally, the best scoring (i.e., with the lowest docking energy or more populated) docked model was chosen to represent the most probable binding mode predicted.

<H1>3. Results and discussion

<H2>3.1. ZnO NPs Characterization

The crystalline nature and phase purity of the synthesized ZnO NPs were analysed using X-ray diffraction (XRD) method. Figure 1a show that the most intense peaks corresponding to (100), (002), (101) crystalline planes and the remaining to (102), (110), (103) and (112) planes. All peaks are characteristic of ZnO and confirming the existence of typical wurtzite crystal structure of NPs [23,24]. *TEM images of ZnO in water have shown polycrystalline structures and aggregates formation. ZnO NPs size powder was estimated from free ZnO NPs observed in the images; they were processed with Image J software with approximately 70 particles observed in 7 TEM images and the average diameter founded was 2.75 nm for ZnO NPs powder without BSA (Figure S1).* Raman spectroscopy is a sensible method to measure changes in the crystal

structure and is used to study the introduction of lattice defects in ZnO materials. Figure 1 b and c present the Raman spectra in the range of 60-3500 cm^{-1} for ZnO solid state and aqueous solution, respectively. In Figure 1b, the dominant peak of the spectrum, localized at 437 cm^{-1} is assigned to the E_{2H} mode of the wurtzite hexagonal structure, attributed at displacements of oxygen atoms [25] confirming the crystallinity of ZnO solid. It is known that the spatial confinement into small diameter particles produces a red shift and asymmetric broadening of the E_{2H} mode compared to bulk crystals that appeared at 435cm^{-1} [26]. In our results, a shift of 2 cm^{-1} for this mode, indicates the presence of particles with size about 4 nm, as was reported by Calizo et al. for ZnO quantum dots [26]. It result is in the same magnitude order than the ZnO NPs size estimated from TEM data. The other bands observed at 98 cm^{-1} (E_{2L} mode), 204 cm^{-1} ($2E_{2L}$ mode), 332 cm^{-1} (second order acoustic mode E_{2H}-E_{2L}) and 380 cm^{-1} A_1 (TO), confirm of wurtzite crystal structure [27]. Furthermore, the bands at 581 cm^{-1} indicate the presence of defects such as zinc interstitials and oxygen vacancies [28], while that the 204 cm^{-1} and 538 cm^{-1} Raman bands confirms of spherical particles formation [27].

On the other hand no characteristic bands were observed in aqueous solution Raman spectra (Figure 1c) in this experimental conditions. Only two peaks at 843 cm^{-1} and 1044 cm^{-1} could be observed. Those results would suggest the aggregates formation in aqueous solution.

The UV–visible spectra of synthesized ZnO nanostructures suspended in water showed a band at 367 nm (3.40 eV), which is blue shifted compared to bulk ZnO, indicating the presence of quantum confinement effects [29].

Figure 2a shows the ZnO NPs in solid phase and aqueous solution emission spectra. Under λ_{exc}=340 nm excitation, the emission spectrum (black solid line) exhibit a dominant band at around 400 nm accompanied by a band in the blue region (455 nm) and other in the green region localized at 520 nm. These emitting wavelengths remain completely unchanged in their shape and position under λ_{exc}=370 nm excitation (black dashed line) except by 400nm band because of the wavelength of excitation. Comparatively, in aqueous solution (Figure 2 b) a new band appears at 425 nm (oxygen vacancies), a red-shift from 520 to 570 nm and a slight decrease in green emission intensity was observed, confirming an increment in the size of the particle into the solution [30].

As ZnO has a broad-band absorption, the excitation spectrum is really important to find the excitation wavelengths at which it has the maximum emission. The excitation spectra of the typical green and blue emission for ZnO NPs solid state and aqueous solution samples were measured and shown in Figure 2c and 2d, respectively. For the typical green emission (550 nm), the excitation spectra for two samples exhibited a band at 365-370 nm (light grey solid line), indicating that the preferential excitation energy is near bandgap. Similar results were obtained for blue emission (450 nm) of solid ZnO, while in solution exhibited a band at about 390 nm in the deep UV region (black solid line). For 400 nm violet emission, the excitation spectra exhibited a weak band at 330 nm for solid compound and 350 nm in solution sample (dark grey line). On one hand, these results are in agreement with violet and blue emission attributed to the transition from extended Zn_i and extended Zn_i states to the valence band [31]. On the other hand, a red-shift from 330 nm (solid phase) to 350 nm (aqueous solution) (Figure 2c and d) under excitation in the UV emission band at 400 nm, indicated a particle size increase in solution.

In contrast to the UV spectra, visible fluorescence spectra of ZnO particles are sensitive to the size. The analysis of the emission spectra using long-pass filters shows that the green band is more defined in aqueous solution and appears slightly red-shifted (Figure S2).
Taking into account these results (Figure S2), we confirmed the aggregation of ZnO NPs in solution. Also, the nanostructured materials are characterized by a high surface to volume ratio, which leads to a large surface area and a concomitant high density of oxygen vacancies, as indicated by the pronounced green PL contribution [32]. Zeng *et. al*.[33] have been attributed a deep-level emission in the green band in highly crystalline particles. *In view of ZnO NP characterization, we asserted the size, crystalline structure and spherical shape for ZnO NPs synthetized by us. Taking into account those results, for the experimental further studies, to avoid NP aggregation, we sonicated previously the NPs solutions.*

<H2>3.2. ZnO NPs emission properties in presence of BSA

The absorbance and fluorescence spectra of ZnO NPs as a function of protein concentration were assayed. The Inset in Figure 3a shows a gradual decreasing in absorbance intensity of ZnO peak at 367 nm with different BSA concentration indicating the presence of BSA on ZnO surface. The spectra exhibit a strong absorption below 400 nm and is consistent with previous reports for colloidal ZnO NP, suggesting their use as an anti-ultraviolet material [34].
Corrected emission spectra at 370 nm (*inset Figure 3b*), before BSA interaction, showed a strong and broad visible emission centred at 565 nm, as well as two weak emission peaks at 425 nm and 450 nm. After conjugation with BSA, visible and ultraviolet emissions of ZnO NPs decreases, and this effect was enhanced with the increased BSA concentration (Figure 3b). An opposite trend for the intensity by violet and blue emission bands centred at 425 nm and 450 nm, respectively, was observed. For BSA concentration higher than 30 μM the overlap between 425 nm signal (oxygen vacancies) and 450 nm (BSA self-oligomerization) was observed. According to the previous results, the functionalization ZnO NPs should be done using diluted BSA solution (< 30 μM).

<H2>3.3. BSA adsorption on ZnO NPs surface

3.3.1.-For the evaluation of the amount of adsorbed protein on ZnO NPs surface, we studied the Trp emission (λexc=295 nm) at 340 nm observed for the BSA with and without ZnO NPs after incubation and centrifugation. The results indicate that the NP emission is practically independent of the BSA concentration to 5 μM of protein (Figure 4), suggesting the formation of a protein-ZnO NP complex. Thus, the Trp emission of the pellets re-suspended in water confirm those results. The analysis of our experiments inferred the absorption of about one protein molecule per single nanoparticle at initial BSA concentration of 5 μM (Figure 4).
3.3.2.-*Other techniques used to evaluate the adsorption of BSA on ZnO NP pellets was supported by their FTIR (ATR mode) and Raman spectra as follows (a) solid ZnO NPs (dried at room temperature), (b) solid BSA (dried at room temperature) c) solid ZnO Nps-BSA conjugated (centrifugated and dried nanoparticles) (c) (See Figure 5).*
On the left FTIR spectrum (a) doesn´t show any significance band, it corresponds to pure NPs, In infrared spectrum of BSA (b) sample two main components (strong bands) are present at 1655 cm^{-1} and. 1545 cm^{-1} corresponding to Amide I and Amide II bands, respectively. The absorption bands at 1653 cm^{-1}, 1545 cm^{-1} and 1384 cm^{-1} correspond to amide I, Amide II and Amide III modes, respectively (c). These bands exhibit a complex band contour and lower intensity than the pure BSA. From the above data we confirm the presence of BSA onto the surface of ZnO NP. On the right Raman spectra, we can see at lower frequencies (600-300 cm^{-1}) spectrum (a) a

characteristic band of ZnO NP. Moreover, spectrum (c) doesn´t change at lower frequencies but new intense bands appear closely at 2800, 1650 and 1540 cm^{-1} are typical of protein.

<H2>3.4. Conformational changes of BSA

To evaluate the conformational changes in the protein structure due to ZnO NP presence, FTIR, Raman and fluorescence spectra were evaluated. It was demonstrated that the Infrared and Raman techniques require high sample concentration. This is why, for all the measurements 30 µM of BSA aqueous solution would be used. Under these experimental conditions, the ZnO NP surface is fully covered. The comparison of the Raman spectral pattern of the native folded protein with that of the same protein adsorbed on ZnO NPs surface, showed surface-driven conformational modifications. The BSA and BSA-ZnO conjugated spectra are slightly different in several spectral regions (showed in Figure S5). Upon interaction with NPs surface, changes in the intensity of Tyr residues modes near 1158 cm^{-1}, 854 and 827 cm^{-1} were found. The latter two bands are related H-bonding capacity as acceptor and/or donor [38], while that the intensity ratio (I_{850}/I_{826}) of Tyrosyl bands reflects the average of OH Tyrosyl hydrogen-bonding states [36]. In our spectra, that ratio is 1.87 and 1.47 for BSA and BSA-ZnO NPs respectively, indicating that in the conjugate ZnO-BSA, Tyr could be acting as a hydrogen-bond donor.

In addition, the comparison of the skeletal stretching mode at 940 cm^{-l} attributed to the α-helical content of protein, suggests that the changes of this signal may be due to slight loss of α-helical content [37]. Slightly changes at 1248 cm^{-1} band, is indicative of grown in the β-sheet [40] structure because of the protein interaction with NPs surface. The combination of these intensity changes at the 1248 cm^{-1} and 940 cm^{-1} lines provides a measure of the α-helical-disordered transformation.

Raman technique has been extensively employed to evaluate the conformation of disulfide bridges in proteins and peptides because the frequency of an S-S stretching mode of the disulfide bridge is sensitive to its conformation. The S-S characteristic frequency occurs at 503 cm^{-1} in BSA and with a noticeably wider half-width [35]. In figure S7 we have been able of identifying two disulfides stretching bands at 507 cm^{-1} and 521 cm^{-1} for Raman BSA spectrum with and without ZnO NPs. The ratio of peak intensities at 507 cm^{-1} and 521 cm^{-1} (I_{521}/I_{507}) in the native BSA is 0.70, indicating that about 12 out of 17 disulfide bridges of the molecules take *ggg* conformation. This value decreased to 0.52 by ZnO NPs interaction, thus, the *ggg* conformation of the disulfide bridges in the BSA was converted to the *ggt* [35]. These results are indicative of conformational changes in the Cys residues by interaction with the ZnO surface.

Perturbations in the protein secondary structure are also confirmed by FTIR spectroscopy (Figure 7). *In order to obtain the relative amounts of different types of secondary structures, the Amide I peak was curve-fitted using the Bruker OPUS 7.0 software. A mixing of Gaussian and Lorentzian function was employed to deconvolute the Amide I band into its constituent vibration modes. The positions of the constituent bands were held fixed, while the intensities and bandwidths were allowed to vary. From the area under the fitted curves, the relative fractions of α-helices, β-sheets, and random coils were determined. According to the literature [6],* the deconvoluted spectra of BSA protein only exhibited α-helix bands since it has 75 % α-helices with very little random coil (~6 %) and β-sheet (~6 %). The BSA-ZnO conjugated exhibits a slight decrease in the relative fraction of α –helices (~67%), together with an increase in β -sheets (~20%). In other words, going from a state free to NPs conjugate, the secondary structure of the BSA changes from α –helix to a β -sheet structure. However, these slight changes indicate that α-helix was retained after the addition of nanostructure, probably because the high curvature of the oxide surface greatly favours the retention of the structure of the protein.

Finally, to confirm conformational changes on BSA structure fluorescence spectra were analysed. Illustrated in Figure 6a are emission spectra of BSA with and without ZnO NPs under excitation at 295 nm. To evaluate the binding site interaction, the environment of the intrinsic tryptophan (Trp) and tyrosine (Tyr) fluorophores were analysed. The BSA emission maximum (340 nm) is blue-shifted when concentration lower than 10 µM BSA were used. *Militello et al. (2003), reported that the peak emission at 340 nm is, principally, due to Trp-134, so the blue-shifted of this emission maximum would indicate that at low concentrations, the interaction with ZnO-NP change the environment of Trp-134, until the more hydrophobic surrounding, indicating rearrangement in the domain I in protein surface. However, at higher concentrations of protein, the NPs surface is covered and the signal obtained is due to protein aggregation* [39].
In Figure 5b, we applied an approach based on the deconvolution of the emission spectra with excitation at 280 nm and 295 nm to analyse conformational transitions induced by ligand binding, as proposed by Bobone *et. al*.[36]. Deconvoluted Fluorescence spectra obtained as a function of ZnO NPs concentrations exhibited a slight increment maximum of band at 305 nm, and it was interpreted as due to the Tyr-Trp energy transfer reduction [37]. Hence, the observed gradual increase in Tyr fluorescence would indicate an increment in rigidity of Tyr moieties and in general a conformational rearrangement of albumin. Furthermore, the changes in the Trp fluorescence as a function of ZnO NPs concentration confirm the interaction of ZnO-NP with IB domain protein structure in which Trp 134 is involved.
The analysis of the difference absorption spectra of BSA with the ZnO NPs contribution subtracted shows a new band at 290 nm, due to the formation ground state complex (inset in Figure S4). In order to study proximity between ZnO NPs binding sites and Trp residues of BSA, changes in intrinsic fluorescence spectra with increasing NP concentration, were evaluated. A gradual decrease of fluorescence of BSA for addition of ZnO NP was observed, indicating a possible quenching (see Figure S5) and a Stern – Volmer constant close to $1.017 \times 10^4\ M^{-1}$ and with a calculated quenching rate constant K_q of $1{,}017 \times 10^{12}\ M^{-1}\ s^{-1}$ (Figure S5). This result indicates that the interaction was through static quenching process, which may be explained by the formation of a complex.
<H2>3.5. Dynamic light scattering analysis

The analysis of hydrodynamic diameter is useful to determine the behaviour of nanoparticle dispersed in water and give us information about aggregation on changing concentrations of NPs. For this essay, we use ZnO NP free powder and ZnO-BSA complex. The average hydrodynamic sizes (Figure 8a) shows a proportional relationship between average diameter and concentration. The higher concentration evaluated (340 µM) showed aggregation while the hydrodynamic diameters observed at 120 µM and 14 µM were 4.4 and 3.5 nm respectively, these values are in the same order of magnitude than those values previously obtained by our TEM micrographs. Therefore it is possible to assume that ZnO-BSA NPs are not aggregated up to concentration observed (120 µM).
The ZnO-BSA complex was obtained mixing 30 mg ZnO dried with 3mL of 5µM BSA after identifying the limit under of which there are not protein aggregation (< 30 µM). DLS measurements of ZnO-BSA NPs at 120µM showed size of 13 nm (Fig 8b). It is worth highlighting that the difference between the hydrodynamic diameter of ZnO NP and ZnO- BSA NP at 120 µM in aqueous solutions is close to 8.5 nm which is nearby of BSA diameter given by the DLS equipment (standard patron), indicating the possibility of a relationship 1:1 in the ZnO-BSA complex. However, at higher concentration (350 µM) showed aggregation despite 15 minutes sonication and the measurement was not reliable (Supplemental material Fig S7).

The smaller size improve ZnO-NP properties but some studies show that nanoparticles smaller than 10 nm can induce cytotoxicity [42,43]. *Taking to account that threshold for first pass elimination by the kidney is estimated to be 10 nm, it is important remark that aggregation produced by protein can change the size of nanoparticles and improve their biocompatibility* [4]. *The tendency of particles to form aggregates depends on the surface charge, the concentration of NP in the reaction media and in the particular case of BSA, it may be possible that hydrophobic and electrostatic interactions between side chains of amino acids driven the agglomeration to form bigger particles as soft corona protein* [44]

<H2>3.6. Domain environment of BSA under ZnO NPs interaction

To our knowledge, this is the first time that a ZnO cluster is used to modelling the nanoparticle. *For a comparative study four clusters has been generated as follows: cluster I for diameter of 1.5 nm; cluster II for diameter of 2.7 nm, cluster III for a surface of 15 Å x 25 Å and cluster IV for a surface of 37 Å x 23 Å.* To determine the contribution of site specific binding amino acids, the possible conformations of the BSA-ZnO complex were calculated. These approaches for docking experiments was validated and consolidated by Khan et al. [17]

First results about binding energy predicted for all BSA-ZnO complex indicate that the IB and IIA subdomains were mostly populated with binding lower energy so these regions were selected as the most probable binding site (Figure 8). *Negatives binding energies of all the ZnO NP-BSA structures show an efficient formation of protein-nanoparticle complexes, being the most stable docked complex the II cluster (Diameter 2.7 nm - Figure 8b). This complex was the most populated cluster with 82 conformations and it had the most binding energy (-12.58 kcal/mol) and intermolecular energy (-14.67 kcal/mol) indicating a strong interaction ZnO- protein. This result is in agree with the experimental size observed from TEM analysis.*

Docking studies suggest that for all the selected structures for this study, the polar interaction plays the main role within a radius of 5 Å, and ZnO NP binds more effectively with ionic groups of amino acids such as Lysine, Glutamic acid, aspartic acid, and glycine residues but low affinity with aromatics amino acids. *Interestingly, the docking evaluation indicated that ZnO does not bind with methionine and Cysteine residues; probably the sulfur atom of chain R group is more blocked to experiment the hydrogen bond* [45]. *This result is according to Raman S-S disulphide analysis that shows slightly changes in the orientation of this group*. Taking to account nanoparticle size, when BSA interacts with smaller ZnO clusters of a.c. 1.5 nm diameter, docking results suggested that six residues (Gln154, Gly162, Asp151, Asn158, Glu284, Pro281) localized in IB and IIA binding domains were attached to the ZnO NP surface to 5 Å of distance. An increment in the size of NP surface (Figure 8, cluster II and III) showed interaction with protein Sudlow´s site I (subdomain IIA) with preference to contact with polar residues. In these structures, the interaction between ZnO NP with BSA structure, changed the calculated partial charge from -16 by BSA alone to 0 by ZnO NP-BSA. For longer surfaces (IV complex), molecular docking studies suggest an adjustment of ZnO NP to IA domain of the protein where the contact residues are mainly ionic nature and non-polar. These results are comparable with those obtained for Khan et al. by HSA-GNP interaction [42]. A detailed result for each ZnO NP binding with residues of BSA interaction site is presented in Table 1.

In order to characterize the binding site of ZnO NP-BSA, we analyzed the cluster II. For this, a further exploration was carried out with a smaller grid map of 60 × 52 × 60 points centered at 18.422, 45.14, and 101.949 with a spacing of 0.375 ˚A. We found that the BSA was binding across of three positives residues (Lys187, Lys294, Lys439), two negatives residues (Glu186 and Glu291) and two neutral polar residues (Tyr451 and Thr190). Interestingly, as shown in Figure

9, docking results infer that the ZnO NP were very nearly attached to the IB and IIA domains localized in the Sudlow´s site I of the protein, where the main residues are ionic or polar. Sudlow´s site I is the preferred to linkage bulky heterocyclic anions whereas Sudlow´s site II is preferred to aromatic carboxylates. Docking analysis revealed that the oxygen atom on ZnO NP and the residues Arg435 and Lys187 are in close proximity (Fig. 9) oriented to hydrogen bonding interactions with Nitrogen atoms (-NH- and -NH_3+- respectively). The orientation of amino acids residues agrees with the established concept that the carboxylate groups side chains strongly coordinate on the NP surface to form a robust coating. Those results would explain the irreversible binding of BSA on ZnO NP surface across of polar interactions, as showed in ZnO-BSA NP Raman spectra, before mentioned. It is possible the biocompatibilization of ZnO for its vehiculization in the bloodstream. On the other hand, taking into account that Sudlow´s site I is occupied by ZnO NP, it is possible to suggest that ZnO-BSA conjugated is suitable to drug delivery for structures similar to ibuprofen molecules which prefer binding to the free Sudlow´s site II [41].

<H2>3.7. Haemolytic activity

In order to secure the results, all the experiments were repeated by triplicated. Both ZnO NPs and BSA modified ZnO exhibited a similar cytotoxicity using 0.5 and 1 mg of ZnO NPs solid. That results confirm a cytotoxicity lower than 0.1% for our ZnO synthetized NP in the experimental condition of this study. In essence, the ZnO and ZnO-BSA NP synthetized in moderate conditions in aqueous medium can be considered as biocompatible, being promise for biological application.

<H2>3.8. BSA esterase-like activity

The retention of BSA activity is of particular importance for any biological application involving nanoparticles. The reactivity of BSA with *p*-nitrophenol acetate is due to their nucleophilic amino acid side chain groups, which hydrolyse *p*-nitrophenyl acetate to produce *p*-nitrophenol with typical absorbance in 405 nm [43–45]. We observed that BSA increments its original activity by ZnO NPs conjugation (Figure 10), probably due to a better accessibility of substrate into the active site due to the molecular rearrangements that suffered the protein. With the ZnO NPs addition, an increment about 50 % in the esterase-like activity was observed, *confirming the assay done by Bhogale et al., 2015* [51] *about improve esterase-like activity of BSA in presence of ZnO.* The assay shows two different behaviour. For a lower concentration of BSA (<30 µM) in the presence of ZnO NP, there is an increase in esterase-like activity, which is in agree on the interaction with *ZnO NP in the binding site I (Domain IIA) that induce rearrangements in the native BSA, more exactly in the environment of site II (subdomain IIIA) which is the active site for p-NPA binding [46]*. *O*n the other hand, for the higher concentration of BSA (>30 µM) in the presence of ZnO NP (Figure S9), there is a decrease in the activity. It can be due to agglomeration effect of albumin at high BSA concentration that decrease to the access to the hydrophobic pocket in the active site [47]. Those results showed that the binding of ZnO NPs to BSA enhanced their activity, indicating a possible improvement in the facilitate transport of fatty acids, including drugs.

<H2>3.9. Thermal stability study

Thermal stability of BSA with ZnO NPs was analysed. NPs possess an enormous surface area and are found to influence the denaturation and amyloid-forming behaviour of proteins very controversially. The interaction of nanoparticles with proteins can affect both protein structure and function; ie, they can inhibit or facilitate amyloid formation. Our previous results showed the BSA reaches a slightly more open structure at the ZnO surface, for this reason, their

consequences on stability were evaluated. From the intrinsic Trp emission monitored by an increase-decrease cycle of the temperature (from 24 °C to 85 °C), was possible to observe a sigmoidal unfolding trend as a function of temperature as shown in Figure 11. The thermal denaturation of BSA followed the same trend in the presence of ZnO NPs with respect to a solution of BSA in buffer. A point of inflexion appeared at approximately 57 °C for the protein, which is shifted to 65 °C in the presence of NPs, which is close to the unfolding mid-point of (T_m= 62.1 °C) found for human serum albumin. Probably, those changes in the transition temperature would be attributed to further polar or electrostatic interaction, which can weaken the tertiary protein structure in agreeing with an increase β-sheet by ZnO NPs- conjugated observed from FTIR spectra (Fig7). Consequently, more energy is needed to unfold the protein. So, we can conclude that upon interaction with ZnO NP, the protein significantly increases its thermal stability and seems to adopt a β-sheet structure in folded state. Moreover this phenomenon may be attributed to ZnO affinity toward the polar residues, that stabilise the molten globule state of the protein and, as a result, aggregation is prevented.
Such thermal stability is important for the enzymatic activity test of same protein binding to the ZnO-BSA NP. This surface offers multiple adsorption points in which hydrogen and ionic interaction could serve as an anchorage of the other molecules of biological interesting.

<H1>4. Conclusions

In summary, we studied the characteristic of the main residues involved in the interaction between BSA and ZnO NPs. The conjugation favoured the thermal stability and esterase-like activity of the protein. Docking results using different NP size indicate that for all analysed NPs, the electrostatic are the main force of interaction; also the simulation showed that 2.5 nm ZnO-NP interacted with polar and ionic residues into IB and IIA subdomains. The emission properties of synthetized ZnO NP at moderate temperature showed green and blue emission and were conserved after protein conjugation with diluted BSA solutions (up to 30 µM). Our results demonstrate that slight conformational changes allow the accommodation of the protein on ZnO NP surface across the IB and IIA subdomains being this site the most likely candidate for thermal stabilization or for fatty acids binding. These ideas facilitate de understanding of nanoparticle-induced protein conformational change and the potential application of the nanoparticle. Because of this study is clearly important to suggest that ZnO NPs with a resistant and biocompatible BSA shell could be used to provide a platform to link other protein or molecules of biological interesting specially for sensors application.

Acknowledgments

We thank Dr. Claudio D. Borsarelli (INBIONATEC-CONICET-UNSE) for the use of the equipment available in his laboratory. We thank our colleague Lic. Pablo Argañaraz for his skillful technical assistance in the registration of DSL data. The authors thank to CCT-CONICET Bahia Blanca for TEM image, CCT-CONICET Tucuman for Raman spectra and CCT-CONICET San Luis for DXR measurements.

Funding Sources

This work was supported by the CONICET (PIP 2012- 2014 GI 11220110100374, PIO-UNSE) and CICyT-UNSE (23/a163).

<REF>References

<BIBL>

[1] I.K. Deshapriya, B.S. Stromer, A. Pattammattel, C.S. Kim, R. Iglesias-Bartolome, L. Gonzalez-Fajardo, V. Patel, J.S. Gutkind, X. Lu, C.V. Kumar,;1; Fluorescent, Bioactive Protein Nanoparticles (Prodots) for Rapid, Improved Cellular Uptake, Bioconjug. Chem. 26 (2015) 396–404. <DOI>10.1021/bc500621h.</DOI>

[2] A. Huefner, W. Kuan, R. a Barker, S. Mahajan,;1; Intracellular SERS Nanoprobes For Distinction Of Different Neuronal Cell Types, Nano Lett. 13 (2013) 2463–2470. <DOI>10.1021/nl400448n.</DOI>
[3] J.W. Rasmussen, E. Martinez, P. Louka, D.G. Wingett,;1; Zinc oxide nanoparticles for selective destruction of tumor cells and potential for drug delivery applications, Expert Opin. Drug Deliv. 7 (2010) 1063–1077. <DOI>10.1517/17425247.2010.502560.</DOI>
[4] G. Bisht, S. Rayamajhi,;1; ZnO Nanoparticles: A Promising Anticancer Agent, Nanobiomedicine. 3 (2016) 9. <DOI>10.5772/63437.</DOI>
[5] S.R. Saptarshi, A. Duschl, A.L. Lopata,;1; Interaction of nanoparticles with proteins: relation to bio-reactivity of the nanoparticle, J. Nanobiotechnology. 11 (2013) 26. <DOI>10.1186/1477-3155-11-26.</DOI>
[6] K.A. Majorek, P.J. Porebski, A. Dayal, M.D. Zimmerman, K. Jablonska, A.J. Stewart, M. Chruszcz, W. Minor,;1; Structural and immunologic characterization of bovine, horse, and rabbit serum albumins, Mol. Immunol. 52 (2012) 174–182. <DOI>10.1016/j.molimm.2012.05.011.</DOI>
[7] P. Esfandfar, M. Falahati, A. Saboury,;1; Spectroscopic studies of interaction between CuO nanoparticles and bovine serum albumin, J. Biomol. Struct. Dyn. 34 (2016) 1962–1968. <DOI>10.1080/07391102.2015.1096213.</DOI>
[8] D. Sengupta, B. Mondal, K. Mukherjee,;1; Visible light absorption and photo-sensitizing properties of spinach leaves and beetroot extracted natural dyes, Spectrochim. Acta - Part A Mol. Biomol. Spectrosc. 148 (2015) 85–92. <DOI>10.1016/j.saa.2015.03.120.</DOI>
[9] M. Shoeb, B.R. Singh, J.A. Khan, W. Khan, B.N. Singh, H.B. Singh, A.H. Naqvi,;1; ROS-dependent anticandidal activity of zinc oxide nanoparticles synthesized by using egg albumen as a biotemplate, Nat. Sci. Nanosci. Nanotechnol. 4 (2013) 35015–11. <DOI>10.1088/2043-6262/4/3/035015.</DOI>
[10] A. Alkaladi, A. Abdelazim, M. Afifi,;1; Antidiabetic Activity of Zinc Oxide and Silver Nanoparticles on Streptozotocin-Induced Diabetic Rats, Int. J. Mol. Sci. 15 (2014) 2015–2023. <DOI>10.3390/ijms15022015.</DOI>
[11] D.P. Neveling, T.S. van den Heever, W.J. Perold, L.M.T. Dicks,;1; A nanoforce ZnO nanowire-array biosensor for the detection and quantification of immunoglobulins, Sensors Actuators B Chem. 203 (2014) 102–110. <DOI>10.1016/j.snb.2014.06.076.</DOI>
[12] D. Sodzel, V. Khranovskyy, V. Beni, A.P.F. Turner, R. Viter, M.O. Eriksson, P.-O. Holtz, J.-M. Janot, M. Bechelany, S. Balme, V. Smyntyna, E. Kolesneva, L. Dubovskaya, I. Volotovski, A. Ubelis, R. Yakimova,;1; Continuous sensing of hydrogen peroxide and glucose via quenching of the UV and visible luminescence of ZnO nanoparticles, Microchim. Acta. 182 (2015) 1819–1826. <DOI>10.1007/s00604-015-1493-9.</DOI>
[13] C. Hanley, J. Layne, A. Punnoose, K.M. Reddy, I. Coombs, A. Coombs, K. Feris, D. Wingett,;1; Preferential killing of cancer cells and activated human T cells using ZnO nanoparticles, Nanotechnology. 19 (2008) 295103. <DOI>10.1088/0957-4484/19/29/295103.</DOI>
[14] M. Fazilati,;1; Investigation toxicity properties of zinc oxide nanoparticles on liver enzymes in male rat, Eur. J. Exp. Biol. 3 (2013) 97–103.
[15] D. Sotnikov, A. Zherdev, B. Dzantiev,;1; Development and Application of a Label-Free Fluorescence Method for Determining the Composition of Gold Nanoparticle–Protein Conjugates, Int. J. Mol. Sci. 16 (2014) 907–923. <DOI>10.3390/ijms16010907.</DOI>
[16] D. Das, B.C. Nath, P. Phukon, A. Kalita, S.K. Dolui,;1; Synthesis of ZnO nanoparticles and evaluation of antioxidant and cytotoxic activity, Colloids Surfaces B Biointerfaces. 111 (2013) 556–560. <DOI>10.1016/j.colsurfb.2013.06.041.</DOI>
[17] S. Khan, A. Gupta, C.K. Nandi,;1; Controlling the Fate of Protein Corona by Tuning Surface Properties of Nanoparticles, J. Phys. Chem. Lett. 4 (2013) 3747–3752. <DOI>10.1021/jz401874u.</DOI>
[18] H. Sowa, H. Ahsbahs,;1; High-pressure X-ray investigation of zincite ZnO single crystals using diamond anvils with an improved shape, J. Appl. Crystallogr. 39 (2006) 169–175. <DOI>10.1107/S0021889805042457.</DOI>
[19] S.I. Roy Dennington,;1; Todd Keith, and John Millam, GaussView, Version 5, (2009).
[20] M. J. Frisch; G. W. Trucks; H. B. Schlegel; G. E. Scuseria; M. A. Robb; J. R. Cheeseman; G. Scalmani; V. Barone; B. Mennucci; G. A. Petersson; H. Nakatsuji; M. Caricato; X. Li; H. P. Hratchian; A. F. Izmaylov; J. Bloino; G. Zheng; J. L. Sonnenberg; M. Had,;1; Gaussian 09, Revision E.01, (2009).
[21] Alessandro Pedretti;1; & Giulio Vistoli, VEGA ZZ 3.0.5 ``Drug design Laboratory, (2014). http://nova.disfarm.unimi.it/cms/index.php?Software_projects:VEGA_ZZ:Download <C>(accessed March 19, 2017).</C>
[22] G.M. Morris, R. Huey, W. Lindstrom, M.F. Sanner, R.K. Belew, D.S. Goodsell, A.J. Olson,;1; AutoDock4 and AutoDockTools4: Automated docking with selective receptor flexibility, J. Comput. Chem. 30 (2009) 2785–2791. <DOI>10.1002/jcc.21256.</DOI>

[23] S.A. Ansari, M.M. Khan, M.O. Ansari, J. Lee, M.H. Cho,;1; Biogenic Synthesis, Photocatalytic, and Photoelectrochemical Performance of Ag–ZnO Nanocomposite, J. Phys. Chem. C. 117 (2013) 27023–27030. <DOI>10.1021/jp410063p.</DOI>
[24] S.A. Ansari, M.M. Khan, J. Lee, M.H. Cho,;1; Highly visible light active Ag@ZnO nanocomposites synthesized by gel-combustion route, J. Ind. Eng. Chem. 20 (2014) 1602–1607. <DOI>10.1016/j.jiec.2013.08.006.</DOI>
[25] A. Sahai, N. Goswami,;1; Structural and vibrational properties of ZnO nanoparticles synthesized by the chemical precipitation method, Phys. E Low-Dimensional Syst. Nanostructures. 58 (2014) 130–137. <DOI>10.1016/j.physe.2013.12.009.</DOI>
[26] I. Calizo, K.A. Alim, V.A. Fonoberov, S. Krishnakumar, M. Shamsa, A.A. Balandin, R. Kurtz,;1; Micro-Raman spectroscopic characterization of ZnO quantum dots, nanocrystals and nanowires, in: K.G. Eyink, D.L. Huffaker, F. Szmulowicz (Eds.), Quantum Dots, Part. Nanoclusters IV, International Society for Optics and Photonics, 2007: p. 64810N. <DOI>10.1117/12.713648.</DOI>
[27] A. Stanković, Z. Stojanović, L. Veselinović, S.D. Škapin, I. Bračko, S. Marković, D. Uskoković,;1; ZnO micro and nanocrystals with enhanced visible light absorption, Mater. Sci. Eng. B Solid-State Mater. Adv. Technol. 177 (2012) 1038–1045. <DOI>10.1016/j.mseb.2012.05.013.</DOI>
[28] A. Umar, S.H. Kim, J.H. Kim, Y.B. Hahn,;1; Structural and optical properties of ZnO nanostructures grown on silicon substrate by thermal evaporation process, Mater. Lett. 62 (2008) 167–171. <DOI>10.1016/j.matlet.2007.04.098.</DOI>
[29] S. Repp, E. Erdem,;1; Controlling the exciton energy of zinc oxide (ZnO) quantum dots by changing the confinement conditions, Spectrochim. Acta Part A Mol. Biomol. Spectrosc. 152 (2016) 637–644. <DOI>10.1016/j.saa.2015.01.110.</DOI>
[30] A. Layek, B. Manna, A. Chowdhury,;1; Carrier recombination dynamics through defect states of ZnO nanocrystals: From nanoparticles to nanorods, Chem. Phys. Lett. 539–540 (2012) 133–138. <DOI>10.1016/j.cplett.2012.05.028.</DOI>
[31] S. Fujita, K. Matsuura,;1; Inclusion of Zinc Oxide Nanoparticles into Virus-Like Peptide Nanocapsules Self-Assembled from Viral β-Annulus Peptide, Nanomaterials. 4 (2014) 778–791. <DOI>10.3390/nano4030778.</DOI>
[32] E. Fazio, a. M. Mezzasalma, G. Mondio, F. Neri, R. Saija,;1; ZnO nanostructures produced by laser ablation in water: Optical and structural properties, Appl. Surf. Sci. 272 (2013) 30–35. <DOI>10.1016/j.apsusc.2012.03.087.</DOI>
[33] B.H. Zeng, G. Duan, Y. Li, S. Yang, X. Xu,;1; Blue Luminescence of ZnO Nanoparticles Based on Non-Equilibrium Processes : Defect Origins and Emission Controls, (2010) 561–572. <DOI>10.1002/adfm.200901884.</DOI>
[34] N.P. Sasidharan, P. Chandran, S. Sudheer Khan,;1; Interaction of colloidal zinc oxide nanoparticles with bovine serum albumin and its adsorption isotherms and kinetics, Colloids Surfaces B Biointerfaces. 102 (2013) 195–201. <DOI>10.1016/j.colsurfb.2012.07.034.</DOI>
[35] R.C. Lord, N. Yu,;1; Laser-excited Raman spectroscopy of biomolecules, J. Mol. Biol. 50 (1970) 509–524. <DOI>10.1016/0022-2836(70)90208-1.</DOI>
[36] R. Žukiene, V. Snitka,;1; Zinc oxide nanoparticle and bovine serum albumin interaction and nanoparticles influence on cytotoxicity in vitro, Colloids Surfaces B Biointerfaces. 135 (2015) 316–323. <DOI>10.1016/j.colsurfb.2015.07.054.</DOI>
[37] J. Bandekar,;1; Amide modes and protein conformation, Biochim. Biophys. Acta (BBA)/Protein Struct. Mol. 1120 (1992) 123–143. <DOI>10.1016/0167-4838(92)90261-B.</DOI>
[38] A. Bouhekka, T. Bürgi,;1; In situ ATR-IR spectroscopy study of adsorbed protein: Visible light denaturation of bovine serum albumin on TiO2, Appl. Surf. Sci. 261 (2012) 369–374. <DOI>10.1016/j.apsusc.2012.08.017.</DOI>
[39] V. Militello, V. Vetri, M. Leone,;1; Conformational changes involved in thermal aggregation processes of bovine serum albumin, Biophys. Chem. 105 (2003) 133–141. <DOI>10.1016/S0301-4622(03)00153-4.</DOI>
[40] S. Bobone, M. van de Weert, L. Stella,;1; A reassessment of synchronous fluorescence in the separation of Trp and Tyr contributions in protein emission and in the determination of conformational changes, J. Mol. Struct. 1077 (2014) 68–76. <DOI>10.1016/j.molstruc.2014.01.004.</DOI>
[41] N.G. Zhdanova, E.A. Shirshin, E.G. Maksimov, I.M. Panchishin, A.M. Saletsky, V. V Fadeev,;1; Tyrosine fluorescence probing of the surfactant-induced conformational changes of albumin, Photochem. Photobiol. Sci. 14 (2015) 897–908. <DOI>10.1039/C4PP00432A.</DOI>
[42] A.E. Nel, L. Mädler, D. Velegol, T. Xia, E.M. V Hoek, P. Somasundaran, F. Klaessig, V. Castranova, M. Thompson,;1; Understanding biophysicochemical interactions at the nano–bio interface, Nat. Mater. 8 (2009) 543–557. <DOI>10.1038/nmat2442.</DOI>

[43] L. Shang, K. Nienhaus, G. Nienhaus,;1; Engineered nanoparticles interacting with cells: size matters, J. Nanobiotechnology. 12 (2014) 5. <DOI>10.1186/1477-3155-12-5.</DOI>
[44] Š. Jasmin, J. Amina,;1; A review on Nanoparticle and Protein interaction in biomedical applications, Period. Eng. Nat. Sci. 4 (2016). <DOI>10.21533/pen.v4i2.62. g86.</DOI>
[45] S. Ranjan, N. Dasgupta, S. Chinnappan, C. Ramalingam, A. Kumar,;1; A Novel Approach to Evaluate Titanium Dioxide Nanoparticle–Protein Interaction Through Docking: An Insight into Mechanism of Action, Proc. Natl. Acad. Sci. India Sect. B Biol. Sci. (2015). <DOI>10.1007/s40011-015-0673-z.</DOI>

[46] S. Khan, A. Gupta, A. Chaudhary, C.K. Nandi,;1; Orientational switching of protein conformation as a function of nanoparticle curvature and their geometrical fitting, J. Chem. Phys. 141 (2014) 84707. <DOI>10.1063/1.4893441.</DOI>

[47] J. Theodore Peters,;1; All about albumin, Academic Press, 1995.

[48] J. Córdova, J.D. Ryan, B.B. Boonyaratanakornkit, D.S. Clark,;1; Esterase activity of bovine serum albumin up to 160°C: A new benchmark for biocatalysis, Enzyme Microb. Technol. 42 (2008) 278–283. <DOI>10.1016/j.enzmictec.2007.10.007.</DOI>

[49] O. Phuangsawai, S. Hannongbua, M.P. Gleeson,;1; Elucidating the Origin of the Esterase Activity of Human Serum Albumin Using QM/MM Calculations, J. Phys. Chem. B. 118 (2014) 11886–11894. <DOI>10.1021/jp506629y.</DOI>

[50] S. Chakraborty, P. Joshi, V. Shanker, Z.A. Ansari, S.P. Singh, P. Chakrabarti,;1; Contrasting Effect of Gold Nanoparticles and Nanorods with Different Surface Modifications on the Structure and Activity of Bovine Serum Albumin, Langmuir. 27 (2011) 7722–7731. <DOI>dx.doi.org/10.1021/la200787t.</DOI>

[51] A. Bhogale, A. Nair, N. Patel, A. Miotello, D.C. Kothari,;1; Esterase activity of BSA-ZnO nanoparticle complex, in: 2014: pp. 205–206. <DOI>10.1063/1.4872545.</DOI>

[52] X. Guo, X. Li, Y. Jiang, L. Yi, Q. Wu, H. Chang, X. Diao, Y. Sun, X. Pan, N. Zhou,;1; A spectroscopic study on the interaction between p-nitrophenol and bovine serum albumin, J. Lumin. 149 (2014) 353–360. <DOI>10.1016/j.jlumin.2014.01.036.</DOI>

</BIBL>

<Figure>**Figure 1**. a)-X-Ray diffraction of synthetized ZnO NPs, b)-Raman spectrum of ZnO NPs solid, b)-Raman spectrum of ZnO NPs in aqueous solution.

<Figure>**Figure 2.** PL spectra of solid ZnO NPs (a) and 2 mM ZnO aqueous solution (b) at λexc= 340 nm (dashed line) and λexc= 370 nm (solid line). Excitation spectrum of solid ZnO NPs (c) and 2 mM ZnO aqueous solution (d), for blue and green emission: Em= 400 nm (black line), Em= 450 nm (dark gray line), Em= 550 nm (gray line).

<Figure>**Figure 3.** a)-UV-visible absorption spectra by ZnO NPs aqueous solution (2mM) recorded in range of 300-500 nm as a function of BSA concentration (0-30 μM). b)-emission spectra (λ_{exc} 370 nm) of ZnO NPs treated with different BSA concentrations from 0 to 100 uM. Black line, BSA 30uM

<Figure>Fig. **4**. a)- Number of adsorbed protein molecules on a single nanoparticle on the protein concentration (1-5 μM). b)- Emission spectra of BSA-ZnO NPs pellets re-suspended in ultrapure water (time incubation 2 hs.) as a function of BSA concentration at 370 nm excitation. Inset Trp emission pellets spectra (λ_{exc}= 295 nm).

<Figure>**Figure 5.** Infrared (on the left) and Raman (on the right) spectra of a) solid ZnO NPs (dried at room temperature), (b) solid BSA (dried at room temperature) and (c) solid ZnO Nps-BSA conjugated (centrifugated and dried nanoparticles).

<Figure>**Figure 6**. (a)-Shifts in emission wavelength (λ max) of ZnO 2 mM aqueous solution by the Bovine serum albumin (BSA) addition of. Inset figure: changes in the Trp emission spectra of the BSA solution (1.5 μM)

and ZnO-BSA suspension (2 mM). BSA (Black line) BSA-ZnO NP (Red line). (b)- Difference emission spectra of BSA (5 μM) in the presence of ZnO NPs in the concentration range of 0-30 μM. The inset corresponds to the intensity at 305 nm vs. ZnO NPs concentration.

<Figure>**Figure 7**. Curve-fitted Amide I ATR-FTIR spectra of BSA (hydrated) and BSA-ZnO conjugate showing secondary structure compositions that are dominated by α -helices (>50%).

<Figure>**Figure 8**. DLS measurements. a)- diameter of ZnO NP at different concentration of aqueous solution. b)- comparison of the diameter of ZnO NPs ans ZnO-BSA NPs in 120 μM aqueous solution.

<Figure>**Figure 9**. Interaction binding site of ZnO NPs structures and BSA protein. (a) I complex, (b) II complex, (c) III complex and d) IV complex.

<Figure>**Figure 10**. Binding Site for II complex of ZnO NP-BSA protein. Green line (H-bonding)

<Figure>**Figure 11**. Esterase activity of BSA as ZnO concentration function

<Figure>**Figure 12**. Temperature effect on BSA fluorescence intensity with and without ZnO nanoparticles. The arrows indicate an inflexion point.

Tables

<Table>**Table I.** Amino acid binding in the docked structure with different ZnO clusters

Cluster	Gln	Gly	Asp	Asn	Glu	Pro	Thr	Lys	Arg	Tyr	Leu	His	Ala	Val	Phe
I	+	+	+	+	+	+									
II					+	+	++	+	+	+					
III	+	++	+		++			+			+		+	+	+
IV	+		++			+		++			+	+			+
			+					+							

+ numbers of times of ZnO NPs interacting with each residue

TDENDOFDOCTD